Time-varying K factor of the mm-Wave Vehicular Channel: Velocity, Vibrations and the Road Quality Influence

BLUMENSTEIN, J.; PROKEŠ, A.; VYCHODIL, J.; POSPÍŠIL, M.; MIKULÁŠEK, T.

Proceedings of the 2017 IEEE 28th Annual International Symposium on Personal, Indoor, and Mobile Radio Communications (PIMRC)

eISBN: 978-1-5386-3531-5

DOI: http://dx.doi.org/10.1109/PIMRC.2017.8292755

Accepted manuscript

Time-varying K factor of the mm-Wave Vehicular Channel: Velocity, Vibrations and the Road Quality Influence

Jiri Blumenstein, Ales Prokes, Josef Vychodil, Martin Pospisil and Tomas Mikulasek
The Faculty of Electrical Engineering and Communication, Brno Univ. of Technology, Czech Rep.
email: blumenstein@vutbr.cz

***Abstract*—This paper evaluates real-world intra-vehicle millimeter-wave (mmWave) channel measurements performed in a vehicular environment. Utilizing a correlative time-domain channel sounder, we demonstrate the dependency of the time-varying Rician K factor on the road quality and instantaneous velocity of the measured vehicle. Vibrations caused by the movement of the vehicle together with mechanical properties of the vehicle's chassis leads to a mutual movement of the transmitting (TX) and the receiving (RX) antennas mounted on the front windshield and on the rear quarter window respectively. The channel sounding is performed in a frequency bandwidth from 59.1 GHz to 64 GHz with 50 GS/s sampling frequency.**

I. Introduction

To support a further evolution of wireless communication systems, considering that the demand for higher data rates still increases, the utilization of formerly unconventional and to some extent unused frequency bands is a precondition [1]. Recognized and promising is the millimeter-wave (mmWave) band. Orthodoxly perceived, the mmWave band spans from 30 GHz to 300 GHz. In this contribution we are however limited by our channels sounder to the frequency band from 59.1 GHz to 64 GHz. As determined by spectrum managing authorities, the mmWave band overlaps the unlicensed industrial scientific and medical (ISM) bands and thus it is remarkably attractive for both research and the industry.

Moreover, as seen by many researchers, vehicle-to-vehicle (V2V), vehicle-to-infrastructure (V2I) and in-vehicle communications may be one of the decisive features of the future cooperative self-driving vehicles [2]. Therefore, the V2V channel characterization and modeling is performed in [3], with a bandwidth of 240 MHz and 5.6 GHz carrier frequency, or with a bandwidth of 20 MHz at 2.4 GHz and 5.9 GHz carrier frequencies in [4].

In the field of in-vehicular mmWave channel characterization, there is a number of publications describing a mmWave channel stationarity [5], [6] or providing channel models and spatial maps [7]–[9]. Not only the passenger compartment is characterized, but also for example the engine bay characterization is the contribution of [10].

978-1-5386-3531-5/17/$31.00

Now, the vehicles are often a subject of vibrations, especially while in operation. The amplitude of the vibrations could be in the order of millimeters [11] and it is therefore comparable with the aptly called mmWave wavelength. The effect of antenna vibrations is studied in [12], [13], where number of possible vibration sources is listed. Mainly, the vibrations are caused by an uneven road surface, engine speed (in revolutions per minute) or sound system of the vehicle. In [12], [13], the vibrations are related to a Doppler spread of the sounding signal.

In this contribution, we utilize the datasets introduced in [12] and we evaluate the in-vehicle line-of-sight (LOS) link vibrations influence via the variations of the K factor.

Please note that the representative datasets, more detailed information about the mmWave time-domain channel sounder is available here: http://www.radio.feec.vutbr.cz/GACR-13-38735S/

II. Measurement

In this section we provide a description of the measurement location and the in-house build (from off-the-shelf components) channel sounder together with the theoretical fundamentals of the time-domain channel sounding with correlative real-time processing.

A. Principle of the correlative channel sounder

The utilized correlative channel sounder measures the transmission channel in the time domain. Other possibility to perform the channel sounding is to utilize the frequency domain channel sounders, where the sounder usually needs some time to sweep the band of interest. Subsequently, sounder stores the channel transfer functions [14]. In the time domain channel sounding, a broadband pulse or sequence is transmitted and the need for the channel sweep time is reduced. Therefore, the time domain channel sounding is suitable for time-variant channels, which is the case of our measured scenario.

(a) The dashboard of the measurement vehicle. Behind the absorbers is the RX with both the up/down Sivers IMA converters and the LNA.

(b) The trunk of the vehicle with the UPS power supply (good for around 1 hour of operation) and DC power supply for LNA and PA.

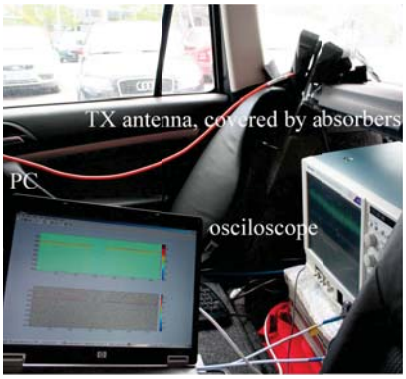

(c) The back seat. The TX antenna is fastened on the rear quarter window using a suction cap. The PA and the is covered by absorbers.

Fig. 1: Measurement setup pictures.

The time-variant channel is described by the channel impulse response (CIR) and is written as [15]:

$$h_m(t,\tau) = \sum_{n=1}^{N(t)} \alpha_n(t) e^{j2\pi f t} \delta\left(\tau - \tau_n(t)\right), \qquad (1)$$

where m is a measurement index and N is the number of propagation paths. The meaning of the measurement index is clarified in section II-B. Note that in this measurement campaign, due to the antenna installation, we ensured that the LOS components $h_{m\mathrm{LOS}}(t,\tau)$ are always present. The summation with the multipath components (MPCs) $h_{m\mathrm{MPC}}(t,\tau)$, i.e.:

$$h_m(t,\tau) = h_{m\mathrm{LOS}}(t,\tau) + h_{m\mathrm{MPC}}(t,\tau), \qquad (2)$$

creates alternative formula to (1).

The correlative channel sounding usually utilizes a properties of pseudo-noise sequences. In this paper, we employ m-sequences [16] with autocorrelation R_{xx} which is, in fact, a sharp triangle function. For our purpose, however, we can simplify to $R_{xx} \approx \delta(\tau)$. Thus, it is possible to write:

$$y(t) = h(t) \otimes x(t), \qquad (3)$$

where $y(t)$ is the received signal, $x(t)$ represents the transmitted m-sequence and finally $\otimes$ stands for a convolution.

Since the index of the transmitted m-sequence is known to the receiver, it is possible to estimate the CIR from the cross-correlation of the transmitted and received signals $x(t)$ and $y(t)$ respectively due to:

$$R_{xy}(\tau) = \mathrm{E}\{x^*(t)y(t)\} = h(t) \otimes R_{xx}(\tau) \approx$$

$$\approx h(t) \otimes \delta(\tau) = h(t), \qquad (4)$$

where $\mathrm{E}\{\}$ stands for the expected value operator. The approximate relation (4) is acceptable if conditions listed in [17] are met.

B. Measurement environment

We have utilized a typical European passenger vehicle, the second gen. Skoda Octavia, with a two-liter diesel engine. The pictures from the measurement campaign are shown in Figure 1.

The measurement campaign itself is consisted from number of channel measurements performed solely inside the car, while the car was in motion. For each channel recording, we have registered the instantaneous velocity. Furthermore, using a subjective three-step metric, the quality of the road was assessed by the driver (i.e., for each channel measurement, we have an index evaluating the "bumpiness" of the actual road). Thus, we have three groups of measurements designated as *smooth road*, *semi-bumpy* and *big potholes*.

Since the measurement setup mimics an intra-vehicle communication link with fixed antenna positions and the presence of the LOS is guaranteed by the installation, we are able to isolate the effect of the vehicle vibrations on the K factor.

1) Measurement devices: The block scheme of the in-house built channel sounder composed from the off-the-shelf components and measurement devices is visible in Figure 2.

The measurement setup consists of the oscilloscope Tektronix MSO72004C (acting as the RX) which was used as the matched receiver with 50 GS/s sampling frequency and 16 GHz bandwidth. The Anritsu Signal Quality Analyzer MP1800A (used as the TX) generates the m-sequences with 13 dBm output power and data rate 12.5 Gbit/s. To improve the dynamic range, the low-noise and power amplifiers QuinStar QLW-50754530-I2 and QPW-50662330 were used. We also utilized

the Sivers IMA FC1003V/01 up and down converter to move the signal to the band of interest.

2) Real-time data processing: The length of the m-sequences is given by the relation $L = 2^k - 1$, where L is the m-sequence length and k is the order of the m-sequence. In this work, we use $k = 11$, thus $L = 2047$.

Now, taking into account that we employ 50 GS/s sampling frequency and that the internal memory of the oscilloscope is 31.25 MS, we are able to capture $T = 3.246\,\text{s}$ of the transmitted signal into the fast internal memory of the oscilloscope (this represents more than 3000 CIRs snapshot for one measurement). Between each channel snapshot, there is a 1 ms pause required. Data are then uploaded to a PC and post-processed. After that, next measurements could be performed.

3) Note on the measurement index m: Each m index denotes a group of over 3000 CIRs recordings. Each group has the total duration of $T = 3.246\,\text{s}$. In total, we captured $m \in \{1, ..., 50\}$ CIRs groups.

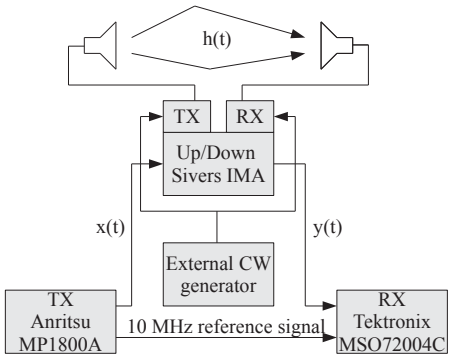

Fig. 2: Time-domain correlative channel sounder utilizing a m-sequence a stable external RF source and a matched receiver.

4) Antennas: The open-ended WR15 waveguide antennas were used at both the RX and TX ends. The radiation patterns are shown in Figure 3.

The TX antenna together with the power amplifier (PA) were mounted on the rear quarter window next to the rear passenger on the right hand side (Fig. 1c). The RX antenna, the low-noise amplifier (LNA) and the up/down converter were fitted approximately in the middle of the dashboard (Fig. 1a). The antennas were attached to the windows with suction caps.

III. Data Acquisition and Processing

A. Rician K factor estimation

The Rician K factor represents the ratio of the specular part r^2 and the variance of the multipath $2\sigma^2$ and is defined in [18] according to

$$K = 10\log_{10}(r^2/2\sigma^2)\ [\text{dB}]. \tag{5}$$

Since the utilized channel sounder is capable to capture the bandwidth of 4.9 GHz, we are not able to adopt the widely applied (e.g. [19], [20]) narrowband

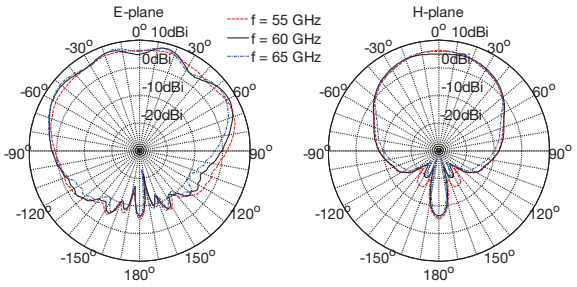

Fig. 3: Measured gain pattern of the open-ended WR15 waveguide in the E–plane and the H–plane for the 55-65 GHz frequency range.

method of moments [21]. We rely on the traditional method for estimation of the K factor from measured power versus time where the LOS component is determined by a peakfinder. Seeing that we measure a fixed link with a single-input single-output (SISO) configuration, the LOS components are always approximately at the same delay bin of the CIR. Therefore, the parametrization of the threshold based method for the estimation of the K factor is straightforward. Then, utilizing (5) and substituting $r(t) = \sum_\tau |h_{\text{LOS}}(t,\tau)|$ and $\sigma(t) = \sum_\tau |h_{\text{MPC}}(t,\tau)|$, we obtain the K factor as a function of time $K_m(t)$.

More detailed information about the channel sounder and how the CIR is obtained from the measured data is available in [13].

1) Decomposition of $K(t)$ into the fast and slow varying components: Based on a visual inspection of the measured data, we operate with a hypothesis that the K factor is composed from two elements according to:

$$K_m^*(t) = K_m(t) + K_m'(t), \tag{6}$$

where $K_m^*(t)$ is the measured K factor, $K_m'(t)$ represents the superimposed fast varying component (noise component) and $K_m(t)$ is the slowly varying component. This is depicted in Figure 4. The decomposition into the slow and fast varying components is done via a discrete wavelet denoising method introduced in [22].

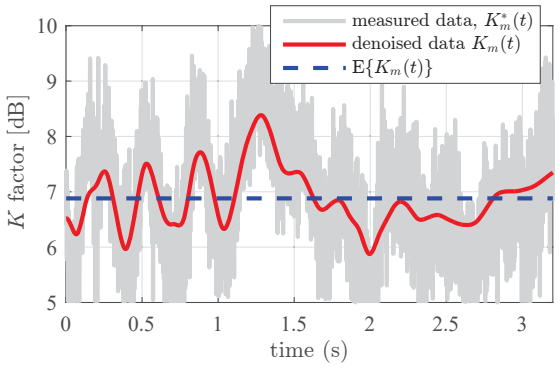

Fig. 4: Example of the K factor evolution in time. The spectrum of the slowly varying signal $K_m(t)$ is further analyzed.

2) Evaluation of the mean K factors: The mean value of the K factor is written as:

$$\mathrm{E}\{K_m(t)\} = \frac{1}{T}\sum_t K_m(t). \tag{7}$$

An example of the mean K factor for one specific measurement index m is depicted in Figure 4. To provide an overview of the mean K factor behavior while driving at variety of speeds and on variety of roads, please see Figure 5. Together with the mean values of the K factor for all measurements m, in Figure 5 we depict a linear fit (written as: $y = kx + c$) obtained by a maximum likelihood estimation (MLE). The values of the parameters k and c are listed in Table I. The interpretation of the results is as follows:

- The higher the speed is, the lower the K factor. It holds namely for the good roads from the group of *smooth surface*.
- If the road quality gets worse (to the level of *semi-bumpy*), the K factor again decreases with increasing speed, however it decreases significantly slower compared to the case of the *smooth surface* group of roads. The reason for this are probably the pronounced vibrations from the road. Interesting is that the *smooth surface* and *semi-bumpy* groups have approximately the same mean K factor for the highest speeds.
- The mean K factors obtained on the worst roads are on similar level as the *semi bumpy*, but we were not able to test all the speeds because the road quality was so poor that we risk damages on the vehicle.

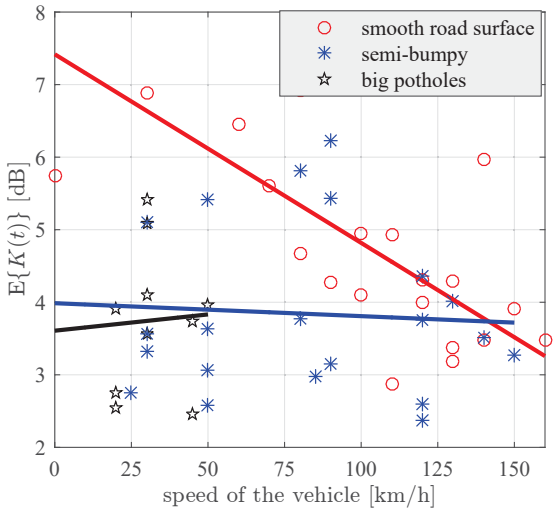

Fig. 5: Mean K factor (over the measurement time T) for all measured datasets $m \in \{1, ...50\}$. Linear fit parameters are listed in Tab. I

3) Analysis of the K factor variations: As demonstrated in Figure 4, the K factor $K_m(t)$ varies with time. Our hypothesis is, that the variations of the K factor are caused by the mechanical vibrations and mutual movement of the RX and TX antennas in general. The mechanical vibrations are related mainly to the road surface quality and vehicle speed. Therefore, utilizing the fast Fourier transform (FFT), we calculate the spectra of all available measurements m according to

$$K_m(f) = \mathrm{FFT}\{K_m(t)\}. \tag{8}$$

The results are plotted in Figure 6, where we also plot the mean spectral values of the representative road quality groups. It is visible, that as the road quality gets worse, the spectrum of the K factor $K_m(f)$ is broadened. In order to evaluate this broadening effect, we introduce a K factor frequency spread metric. The metric is given as a frequency spread, which is observed at the 40 dB decrease of the K factor spectrum $K_m(f)$ from its maximal value.

Now, the results of the K factor frequency spread are plotted in Figure 7 and we conclude that:

- The best road quality produces the lowest spread of the $K_m(f)$ values and the worst road quality produces the highest spread of the $K_m(f)$ values.
- K factor frequency spread increases with the speed.
- $K_m(f)$ spread increases faster as the road quality worsens.

Intuitively, the effect of the increasing speed and worsening of the road quality leads to a vibration increase. The K factor, influenced by a mutual antenna movement and variations of the of the antenna alignment, is shown as indirectly proportional to the vehicle vibrations.

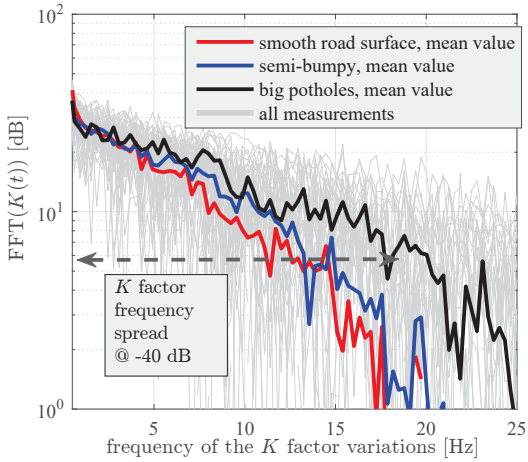

Fig. 6: Spectra of denoised $K(t)$ for all measurements (gray) and spectra of the mean values of the *smooth road*, *semi-bumpy* and *big potholes* groups.

IV. Conclusion

We present the K factor evaluation for variety of road conditions and the velocities of the measured vehicle. Since the measurement setup mimics an intra-vehicle communication link with fixed antenna positions and the

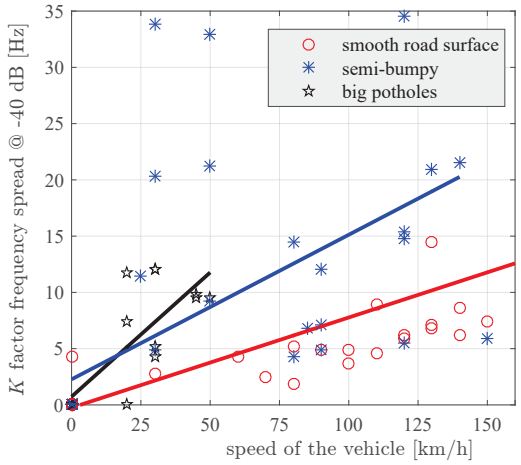

Fig. 7: The frequency spread of the denoised $K(f)$ for all measurements associated to the representative road quality groups.

TABLE I: Linear fit parameters of the of $\mathrm{E}\{K_m(t)\}$ and $\mathrm{FFT}\{K_m(t)\}\forall m$.

	mean K factor		K factor spread	
fit params. of $y = kx + c$ approx.	k	c	k	c
smooth road	-0.0260	7.418	0.0801	-0.248
semi-bumpy	-0.0017	3.987	0.1285	2.273
big potholes	0.0044	3.608	0.2208	0.732

presence of the LOS is guaranteed by the installation, we are able to isolate the effect of the vehicle vibrations. The baseline hypothesis is confirmed, the higher the speed of the vehicle, the lower the mean K factor. Also, the higher the speed, the higher variations of the K factor in the time domain.

The influence of the subjective index of the road quality on the K factor is also evaluated. The results show that as the road worsens, the mean K factor decreases while the frequency of the K factor variations is increased. In the absolute values, the presented results hold for one specific vehicle, one specific channel sounder and on top of that, for one specific test drive. However, the authors reckon that the shown trends will hold also for other (yet similar) vehicles.

Acknowledgment

The research described in this paper was financed by the Czech Science Foundation, Project No. 17-27068S, and by National Sustainability Program under grant LO1401. For the research, the infrastructure of the SIX Center was used.

References

[1] T. S. Rappaport, S. Sun, R. Mayzus, H. Zhao, Y. Azar, K. Wang, G. N. Wong, J. K. Schulz, M. Samimi, and F. Gutierrez, "Millimeter wave mobile communications for 5G cellular: It will work!" *IEEE access*, vol. 1, pp. 335–349, 2013.

[2] C. Sommer and F. Dressler, *Vehicular Networking*. Cambridge University Press, 2014.

[3] T. Abbas, J. Nuckelt, T. Krner, T. Zemen, C. F. Mecklenbruker, and F. Tufvesson, "Simulation and measurement-based vehicle-to-vehicle channel characterization: Accuracy and constraint analysis," *IEEE Transactions on Antennas and Propagation*, vol. 63, no. 7, pp. 3208–3218, July 2015.

[4] M. Boban, T. T. V. Vinhoza, M. Ferreira, J. Barros, and O. K. Tonguz, "Impact of vehicles as obstacles in vehicular ad hoc networks," *IEEE Journal on Selected Areas in Communications*, vol. 29, no. 1, pp. 15–28, January 2011.

[5] J. Blumenstein, A. Prokes, A. Chandra, T. Mikulasek, R. Marsalek, T. Zemen, and C. Mecklenbruker, "In-vehicle channel measurement, characterization, and spatial consistency comparison of 3-11 GHz and 55-65 GHz frequency bands," *IEEE Trans. Veh. Technol.*, vol. 66, no. 5, pp. 3526–3537, May 2017.

[6] J. Blumenstein, T. Mikulasek, R. Marsalek, A. Chandra, A. Prokes, T. Zemen, and C. Mecklenbrauker, "In-vehicle UWB channel measurement, model and spatial stationarity," in *Vehicular Networking Conference (VNC), 2014 IEEE*. IEEE, 2014, pp. 77–80.

[7] J. Blumenstein, T. Mikulasek, R. Marsalek, A. Prokes, T. Zemen, and C. Mecklenbrauker, "In-vehicle mm-wave channel model and measurement," in *Vehicular Technology Conference (VTC Fall), 2014 IEEE 80th*. IEEE, 2014, pp. 1–5.

[8] M. Schack, J. Jemai, R. Piesiewicz, R. Geise, I. Schmidt, and T. Kurner, "Measurements and analysis of an in-car UWB channel," in *Vehicular Technology Conference, 2008. VTC Spring 2008. IEEE*, 2008, pp. 459–463.

[9] J. Blumenstein, T. Mikulasek, R. Marsalek, A. Prokes, T. Zemen, and C. Mecklenbrauker, "Measurements of ultra wide band in-vehicle channel - statistical description and TOA positioning feasibility study," *EURASIP Journal on Wireless Communications and Networking*, p. 15, 2015.

[10] U. Demir, C. Bas, and S. Ergen, "Engine compartment UWB channel model for intravehicular wireless sensor networks," *IEEE Transactions on Vehicular Technology*, vol. 63, no. 6, pp. 2497–2505, July 2014.

[11] S. Lakušić, D. Brčić, and V. Tkalčević Lakušić, "Analysis of vehicle vibrations–new approach to rating pavement condition of urban roads," *PROMET-Traffic & Transportation*, vol. 23, no. 6, pp. 485–494, 2011.

[12] J. Blumenstein, J. Vychodil, M. Pospisil, T. Mikulasek, and A. Prokes, "Effects of vehicle vibrations on mm-wave channel: Doppler spread and correlative channel sounding," in *2016 IEEE 27th Annual International Symposium on Personal, Indoor, and Mobile Radio Communications (PIMRC)*, Sept 2016, pp. 1–5.

[13] A. Prokes, J. Vychodil, M. Pospisil, J. Blumenstein, T. Mikulasek, and A. Chandra, "Time-domain nonstationary intra-car channel measurement in 60 GHz band," in *2016 International Conference on Advanced Technologies for Communications (ATC)*, Oct 2016, pp. 1–6.

[14] A. Chandra, A. Prokes, T. Mikulek, J. Blumenstein, P. Kukolev, T. Zemen, and C. F. Mecklenbruker, "Frequency-domain in-vehicle UWB channel modeling," *IEEE Trans. Veh. Technol.*, vol. 65, no. 6, pp. 3929–3940, June 2016.

[15] F. Hlawatsch and G. Matz, *Wireless communications over rapidly time-varying channels*. Academic Press, 2011.

[16] S. W. Golomb *et al.*, *Shift register sequences*. Aegean Park Press, 1982.

[17] G. Matz, A. F. Molisch, F. Hlawatsch, M. Steinbauer, and I. Gaspard, "On the systematic measurement errors of correlative mobile radio channel sounders," *IEEE Transactions on Communications*, vol. 50, no. 5, pp. 808–821, 2002.

[18] S. O. Rice, "Statistical properties of a sine wave plus random noise," *The Bell System Technical Journal*, vol. 27, no. 1, pp. 109–157, Jan 1948.

[19] A. Bottcher, P. Vary, C. Schneider, M. Narandzic, and R. S. Thoma, "Estimation of the radio channel parameters from a circular array with directional antennas," in *2011 IEEE 73rd Vehicular Technology Conference (VTC Spring)*, May 2011.

[20] L. Bernado, T. Zemen, F. Tufvesson, A. F. Molisch, and C. F. Mecklenbrauker, "Time- and frequency-varying K-factor of non-stationary vehicular channels for safety-relevant scenarios," *IEEE Transactions on Intelligent Transportation Systems*, vol. 16, no. 2, pp. 1007–1017, April 2015.

[21] L. J. Greenstein, D. G. Michelson, and V. Erceg, "Moment-method estimation of the ricean K-factor," *IEEE Communications Letters*, vol. 3, no. 6, pp. 175–176, June 1999.

[22] D. L. Donoho, "De-noising by soft-thresholding," *IEEE Transactions on Information Theory*, vol. 41, no. 3, pp. 613–627, 1995.